AIP | Journal of Applied Physics

Antimony desinsertion reaction from SbxCoSb3−x

F. Miotto, C. A. Figueirêdo, G. R. Ramos, C. L. G. Amorim, M. R. Gallas et al.

Citation: J. Appl. Phys. **110**, 043529 (2011); doi: 10.1063/1.3626045
View online: http://dx.doi.org/10.1063/1.3626045
View Table of Contents: http://jap.aip.org/resource/1/JAPIAU/v110/i4
Published by the American Institute of Physics.

Antimony desinsertion reaction from Sb_xCoSb_{3-x}

F. Miotto,[1] C. A. Figueirêdo,[2] G. R. Ramos,[1] C. L. G. Amorim,[1] M. R. Gallas,[3] and C. A. Perottoni[1,a)]
[1]*Universidade de Caxias do Sul, 95070-560 Caxias do Sul, Rio Grande do Sul, Brazil*
[2]*Universidade Federal do Rio Grande do Sul, PGCIMAT, 91501-970 Porto Alegre, Rio Grande do Sul, Brazil*
[3]*Universidade Federal do Rio Grande do Sul, Instituto de Física, 91501-970 Porto Alegre, RS, Brazil*

(Received 29 March 2011; accepted 5 July 2011; published online 30 August 2011)

The compound $Sb_x CoSb_{3-x}$ was produced at 7.7 GPa and 550 °C in a self-insertion reaction from the binary skutterudite $CoSb_3$. This self-insertion reaction is characterized by the collapse of some framework Sb atoms into the cages formed by the Co and Sb atoms in the skutterudite structure, as was further confirmed by Bader's analysis of maximum-entropy charge density maps obtained from synchrotron radiation x-ray powder diffraction data. The opposite reaction (i.e., Sb desinsertion, $Sb_x CoSb_{3-x} \rightarrow CoSb_3$) occurs when $Sb_x CoSb_{3-x}$ is heated above 180 °C at ambient pressure. This desinsertion reaction was followed by means of differential scanning calorimetry, x-ray diffraction, and electrical resistivity measurements. Differential scanning calorimetry measurements revealed the presence of two thermal events in samples rich in the $Sb_x CoSb_{3-x}$ phase. An endothermic peak around 150 °C was assigned to a small change in the position of the guest Sb atoms inside the cages of $Sb_x CoSb_{3-x}$. This assignment was based on the analysis of charge density maps obtained from synchrotron x-ray diffraction measurements carried out both at room temperature and at 155 °C. Accordingly, the guest Sb atoms in $Sb_x CoSb_{3-x}$ shift from the 12d (x,0,0) site of $Im\bar{3}$ space group (in a position distant about 0.35 Å from the center of the cages), at room temperature, to the 2a (0,0,0) site (i.e., to the center of the cages) above 150 °C. An exothermic event starting at 180 °C is the thermal signature of the desinsertion of guest Sb atoms from the $Sb_x CoSb_{3-x}$ skutterudite cages, as confirmed by x-ray diffraction analysis and further verified by electrical measurements. After heating to 350 °C, $Sb_x CoSb_{3-x}$ samples fully convert back to $CoSb_3$. The Sb desinsertion reaction from $Sb_x CoSb_{3-x}$ follows a first order kinetics, with a transition enthalpy of approximately 21 kJ/mol and an activation energy of 83 kJ/mol. [doi:10.1063/1.3626045]

I. INTRODUCTION

For some time now, skutterudite compounds have been considered as potential candidates for thermoelectric materials with high figure of merit.[1–11] These compounds exhibit cubic crystal structures, with space group $Im\bar{3}$ and general formula $\square MX_3$, where M is a transition metal (Co, Fe, Ir, Rh) occupying site 8c and X = P, As or Sb (site 24 g). The symbol $\square$ represents a vacancy (situated into a cage formed by the atoms in the 8c and 24 g sites), which can be empty or partially occupied by alkaline earth or lanthanide ions.[3–5] To be a useful thermoelectric material, it must have a large thermoelectric figure of merit, defined as $ZT = \alpha^2 T/\rho k$, where α is the Seebeck coefficient, ρ is the electrical resistivity, k is the thermal conductivity, and T is the absolute temperature. Relatively large ZT values, around 2.5 at room temperature, have been obtained for nanostructured thermoelectric materials.[6] By filling the cages in the skutterudite structure with elements that are loosely bound to the framework and are able to *rattle* around the equilibrium position, one have an efficient phonon-scattering mechanism that reduces significantly the lattice thermal conductivity, thus increasing the figure of merit.[5–9,12] Recently, a kind of self-insertion reaction induced by high pressure was observed for the compound $CoSb_3$.[10,11] In fact, at room temperature and above about 20 GPa, cobalt antimonide undergoes an irreversible isosymmetric transition to a phase with molar volume at ambient pressure greater than that of pristine $CoSb_3$. This anomalous behavior was interpreted as a pressure-induced self-insertion reaction, in which antimony atoms from the $CoSb_3$ framework collapses and partially fills the cages formed by Sb and Co atoms. From now on, the phase obtained by self-insertion of Sb into the cages of $CoSb_3$ will be referred to as $Sb_x CoSb_{3-x}$. This self-insertion reaction was also observed at lower pressures and moderate temperatures in experiments carried out in a toroidal high pressure cell. Also, further evidence of this transition has been provided by Matsui *et al*. in a recent study of the pressure behavior of TSb_3 (T = Co, Rh, and Ir).[13]

In this work, samples of $Sb_x CoSb_{3-x}$ were produced at high pressure and high temperature aiming to obtain further insight on the nature of the guest atom. Also, the change with temperature of the crystallographic site occupied by the atoms that collapses into the skutterudite cages was explored by means of model-independent charge density maps derived from synchrotron radiation x-ray powder diffraction data. In fact, in spite we already referred to the high pressure phase as $Sb_x CoSb_{3-x}$, conclusive evidence that Sb atoms actually

a)Electronic mail: caperott@ucs.br.

collapse to the interior of the $CoSb_3$ cages under high pressure will be provided by Bader's analysis of the charge density distribution of the high pressure phase, as will be described in this work. Furthermore, to study the inverse reaction, i.e., the desinsertion of guest atoms from the cages of the $Sb_x CoSb_{3-x}$ skutterudite, samples prepared at high pressure and high temperature were studied at ambient pressure by x-ray powder diffraction, differential scanning calorimetry analysis, and electrical resistivity measurements, both *in situ* and after heating up to 350 °C.

II. EXPERIMENTAL PROCEDURE

The samples of $CoSb_3$ used in this work were prepared from the elements as described in previous works.[11,14] Five different samples of $Sb_x CoSb_{3-x}$ were prepared from $CoSb_3$ in a toroidal-type chamber assembled in a 400 ton hydraulic press. Sample #1 was prepared by submitting $CoSb_3$ to 7.7 GPa and 550 °C for 20 min. Samples #2, #3, #4, and #5 were produced from $CoSb_3$ pre-treated at 2.5 GPa, and 500 °C for 60 min and then were submitted to 7.7 GPa and 550 °C for 60 min in an attempt to increase the relative amount of the $Sb_x CoSb_{3-x}$ phase. Despite all efforts in obtaining single phase $Sb_x CoSb_{3-x}$ samples, this has proven to be unfeasible within the limits of pressure imposed by the toroidal high pressure cell used in this work. In fact, at least two parallel reactions occur when $CoSb_3$ samples are submitted to 7.7 GPa and 550 °C. The first one is the self-insertion reaction already mentioned before. The second one is the decomposition reaction $CoSb_3 \rightarrow CoSb_2 + Sb$, which leaves some contaminant phases ($CoSb_2$ and Sb) present in the samples. The results obtained so far suggest that to produce a sample of $Sb_x CoSb_{3-x}$ free of contaminant phases, it would be necessary to submit $CoSb_3$ samples to pressures higher than 7.7 GPa, while keeping the temperature below 550 °C. As we shall see, the free Sb from the decomposition of $CoSb_3$ also contributes to form $Sb_x CoSb_{3-x}$ at high pressure and high temperature. The phase composition and $Sb_x CoSb_{3-x}$ lattice parameter for the samples used in this work were determined by Rietveld analysis of their x-ray powder diffraction patterns at ambient conditions and are given in Table I.

X-ray powder diffraction patterns were collected using a Shimadzu 6000 diffractometer, with Cu $K\alpha$ radiation ($\lambda = 0.15404$ nm), in the angular range from 12° to 56° (2θ), with a step size of 0.05° and 4 s integration time. The diffractometer was equipped with Soller slits in the incident and diffracted beams, an 1 ° divergence slit, a 0.30 mm receiving slit, and a graphite monochromator in the diffracted beam.

TABLE I. Phase composition and $Sb_x CoSb_{3-x}$ lattice parameter and 2a site fractional occupancy for samples #1 to #5. The figures in parentheses are the uncertainties in the last significant digit.

			$Sb_x CoSb_{3-x}$		
Sample #	$CoSb_2$ (wt%)	$CoSb_3$ (wt%)	(wt%)	a(Å)	Occ.
1	13(1)	2(1)	85(4)	9.127(4)	0.72(6)
2	5(1)	5(2)	90(6)	9.125(1)	0.59(5)
3	7(1)	12(1)	81(3)	9.126(1)	0.63(3)
4	9(1)	15(2)	76(4)	9.126(5)	0.68(5)
5	9(1)	18(2)	73(2)	9.127(1)	0.67(6)

Further angle-dispersive x-ray diffraction measurements of $Sb_x CoSb_{3-x}$ were carried out in the x-ray powder diffraction (XPD) beamline at D10B in the Laboratório Nacional de Luz Síncrotron (LNLS) (Campinas, Brazil).[15] In this experiment, synchrotron radiation was monochromatized by a double-bounce Si(111) monochromator. The wavelength ($\lambda = 0.123\ 857$ nm) was determined from the analysis of the Bragg peaks from a sample of silicon standard (NIST SRM640c). The measurements were performed in $\theta - 2\theta$ geometry, employing a Ge(111) crystal analyzer installed in front of a scintillation detector. Step-scan data were collected over the angular range between 10° and 120° (2θ). The samples, mounted on an aluminum sample holder for measurements at room temperature and on a copper sample holder for measurements at 155 °C, were attached to a goniometer head with four adjustable axes on a Huber $4+2$ circle diffractometer. Measurements at 155 °C and 10^{-5} Pa were carried out with a commercial closed-cycle He cryostat with vibration damping and temperature control. Structural parameters were obtained by Rietveld analysis of the x-ray powder diffraction patterns using the computer program Fullprof.[16,17] Charge density distribution of $Sb_x CoSb_{3-x}$ was determined by the maximum-entropy method (MEM) using the MEM-based pattern fitting (MPF) method, with the programs Rietan-FP and PRIMA.[18–20] Split pseudo-Voigt functions were used to fit Bragg peaks and the peak profile was calculated within $15 \pm$ FWHM (full width at half maximum) of peak position. A Legendre polynomial was fitted to background intensities with 10 adjustable parameters.[21] The unit cell was divided into $100 \times 100 \times 100$ pixels for MPF calculations. In this iterative procedure, the charge density distribution is first calculated from a set of structure factors obtained from Rietveld refinement of the x-ray diffraction pattern. The structural parameters of $CoSb_3$ were used as a starting point for the iterative MPF calculations to avoid any bias toward a pre-defined structural model for $Sb_x CoSb_{3-x}$.[22] The refinement proceeds by calculating the charge density distribution compatible with the set of structure factors that maximize information entropy. A new set of structure factors is thus calculated from this charge density distribution, and this iterative procedure goes on until convergence is achieved. The three-dimensional charge density distribution was visualized as isosurfaces with the computer program VESTA.[23] An estimate of the electronic charge of the guest atom inside the high pressure and high temperature skutterudite cages was obtained from the maximum-entropy charge density distribution according to Bader's theory of atoms in molecules.[24]

A total of 215 structure factors were extracted from the x-ray powder diffraction data, and these were used in the MPF analysis. This relatively small set of structure factors (which was limited by the experimental conditions available at the D10B beamline in the LNLS) imposes a severe limitation on the precise determination of the charge of the guest atom inside the cages of the high pressure phase and also on the detailed mapping of the charge distribution in

$Sb_x CoSb_{3-x}$. Despite these limitations, the synchrotron x-ray powder diffraction data has enough quality as for a conclusive identification of the atom collapsed to the interior of the $CoSb_3$ cages under high pressure. The XPD data also allowed the study of the effect of temperature on the position of the guest atom inside the skutterudite cages.

The desinsertion reaction $Sb_x CoSb_{3-x} \rightarrow CoSb_3$ was followed *in situ* by differential scanning calorimetry analysis (DSC), which was performed with a TA Instruments Q2000 heat flux calorimeter. The $Sb_x CoSb_{3-x}$ sample was placed into a sealed aluminum pan on the sample furnace of the calorimeter and scanned from 10 °C up to 380 °C, at a heating rate of 10 °C/min, using argon as purge gas. The reaction order and activation energy of the desinsertion reaction was estimated by the method of Borchardt and Daniels.[25] Reaction enthalpies and activation energies were corrected for the actual amount of $Sb_x CoSb_{3-x}$ present in the samples, as determined by Rietveld analysis of their x-ray diffraction patterns. Electrical resistivity was measured using a four-point technique suitable for cylindrical samples with high thickness-to-diameter ratio.[26]

III. RESULTS AND DISCUSSION

Figure 1 shows synchrotron radiation x-ray powder diffraction patterns of pristine $CoSb_3$ and $Sb_x CoSb_{3-x}$ (sample #1) at room temperature. The $Sb_x CoSb_{3-x}$ phase is characterized by the displacement of cobalt antimonide Bragg peaks toward lower angles and by the reduction of the intensity of 110, 200, and 211 Bragg peaks.[10] The separation of Bragg peaks from $CoSb_3$ and $Sb_x CoSb_{3-x}$ can be better appreciated in the inset of Fig. 1(a), while the reduction of the intensity of 110, 200, and 211 Bragg peaks can be seen in the inset of Fig. 1(b).

Besides the product from the self-insertion reaction, $CoSb_3 \rightarrow Sb_x CoSb_{3-x}$, one should note in the powder pattern shown in Fig. 1(b) the presence of $CoSb_2$ resultant from a parallel decomposition reaction, $CoSb_3 \rightarrow CoSb_2 + Sb$. However, there is no evidence of free Sb from the decomposition reaction in the x-ray powder diffraction pattern shown in Fig. 1(b). This observation suggests that the Sb resulting from decomposition of $CoSb_3$ at high pressure and high temperature may also be inserted into the cages of cobalt antimonide, thus forming some fraction of the $Sb_x CoSb_{3-x}$ phase present in the sample. A similar behavior was previously observed with tin.[27] Nevertheless, it must be stressed that the insertion reaction of $CoSb_3$ with free Sb cannot account for all $Sb_x CoSb_{3-x}$ formed at high pressure and high temperature, as the amount of the latter in our samples is much greater than it would be expected solely on the basis of the insertion reaction with free Sb formed from $CoSb_3$ decomposition. Also, the amount of free Sb present in the as-synthesized $CoSb_3$ is actually very small (less than 2%wt), as inferred from Rietveld analysis of data shown in Fig. 1(a). Furthermore, in experiments conducted with $CoSb_3$ (and related compounds) at high pressure and room temperature, $Sb_x CoSb_{3-x}$ is observed with no apparent contamination from $CoSb_2$.[10,13] As we shall see, Bragg peaks from free Sb formed by decomposition of $CoSb_3$ will be identified in the x-ray powder diffraction pattern of samples previously rich in $Sb_x CoSb_{3-x}$, after heating to temperatures high enough to promote the desinsertion reaction.

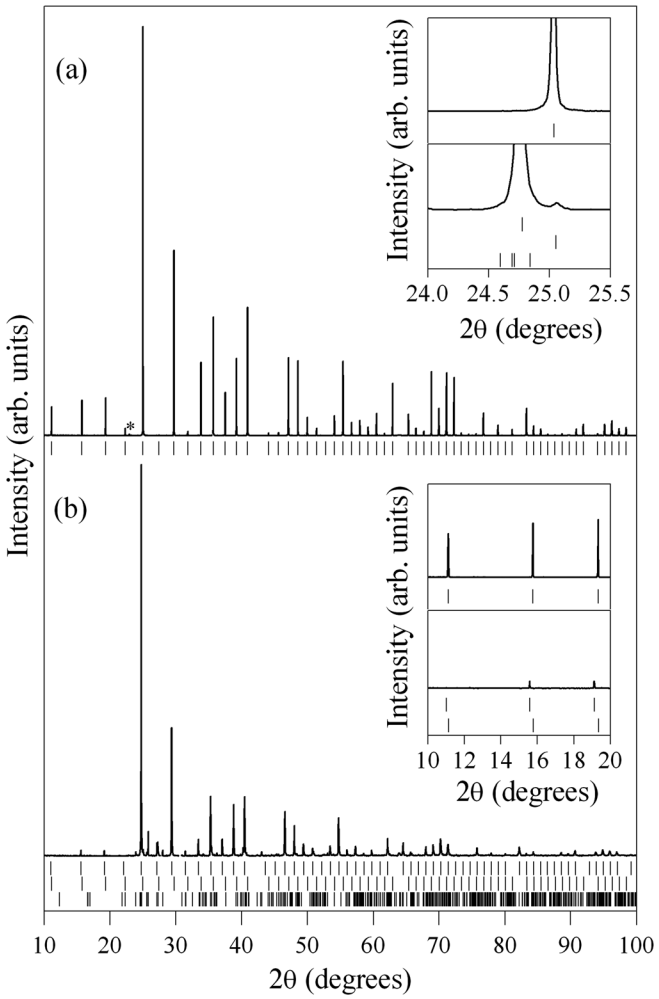

FIG. 1. Synchrotron radiation x-ray powder diffraction patterns of (a) $CoSb_3$ pristine and (b) sample #1, rich in the $Sb_x CoSb_{3-x}$ phase, both at ambient conditions. Intensities were normalized with respect to the amplitude of the (most intense) 310 Bragg peak. The tick marks indicate the expected positions of Bragg peaks from (a) $CoSb_3$ and, in (b), from top to bottom, $Sb_x CoSb_{3-x}$, $CoSb_3$, and $CoSb_2$. The asterisk in (a) signals the expected position of the most intense (012) Bragg peak from Sb. The inset in (a) shows the separation of Bragg peaks from $CoSb_3$ and $Sb_x CoSb_{3-x}$, and the inset in (b) shows the intensity reduction of 110, 200, and 211 Bragg peaks upon Sb insertion at 7.7 GPa and 550 °C. For both insets, the data shown at the top and at the bottom correspond to pristine $CoSb_3$ and to sample #1, respectively.

The room temperature $CoSb_3$ lattice parameter [$a_o = 9.036(2)$ Å] is in good agreement with literature.[8,10,22] On the other hand, the $Sb_x CoSb_{3-x}$ lattice parameter is about 0.011 Å smaller than previously reported.[10] The $Sb_x CoSb_{3-x}$ lattice parameter varies with the actual value of x for each sample. However, the origin of the above-mentioned discrepancy is mainly due to the fact that in our previous work, based on conventional x-ray powder diffraction data, we supposed that the sample consisted of a mix of two $Sb_x CoSb_{3-x}$ phases with distinct 2a site occupancies (two different values of x) and, thus, two slightly distinct lattice parameters. The improved resolution and overall quality of the synchrotron radiation XPD data, shown in Fig. 1, now

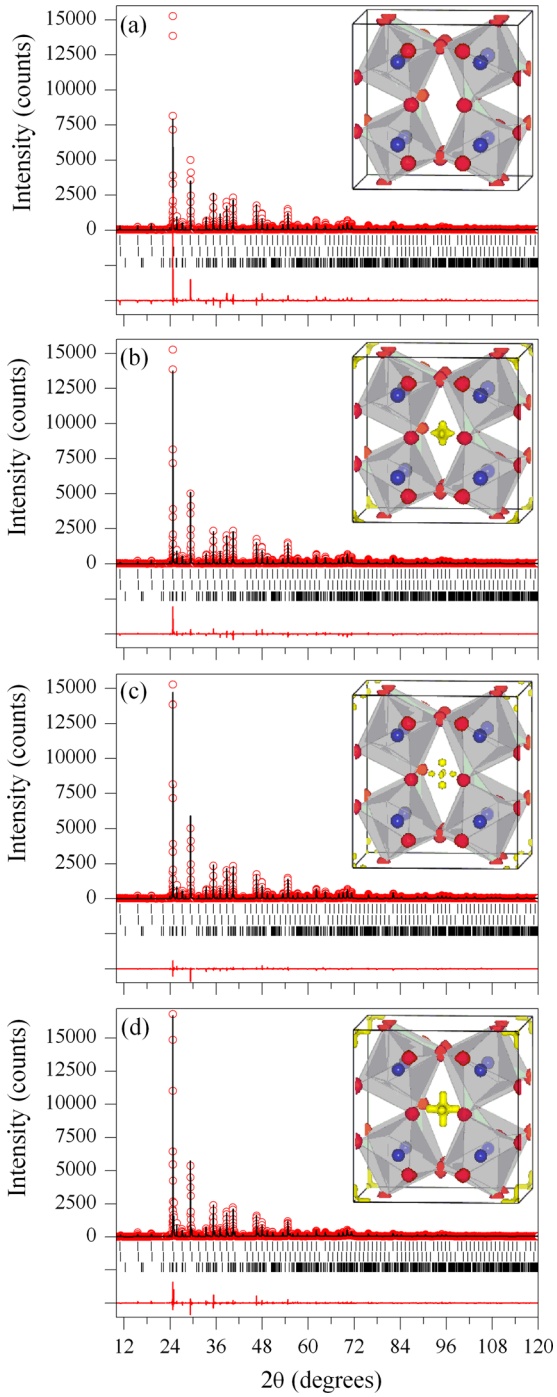

FIG. 2. (Color online) Results from Rietveld refinement (panel a) and MEM-based pattern fitting (panels b-d) for sample #1, and the corresponding charge density isosurfaces for $Sb_x CoSb_{3-x}$ (22 $e/Å^3$) derived from synchrotron x-ray powder diffraction data taken at room temperature (panels a-c) and at 155 °C (panel d). The measured data are shown as red circles, the calculated pattern is the black solid line, and the difference curve is shown below in red. The small vertical tick marks indicate the expected positions of Bragg peaks from $Sb_x CoSb_{3-x}$ (top), $CoSb_3$ (middle), and $CoSb_2$ (bottom). The insets show the three-dimensional charge density isosurfaces for $Sb_x CoSb_{3-x}$, represented in blue and red at the positions occupied by Co and Sb, respectively, in the $CoSb_3$ unit cell. First-coordination $CoSb_6$ polyhedra are represented in gray. Also represented in yellow in the insets are the charge density isosurfaces corresponding to the charge buildup near the center (and at the equivalent positions) of the unit cell for $Sb_x CoSb_{3-x}$ at room temperature (panels b-c) and at 155 °C (panel d). In panel a, the Rietveld refinement was carried out with a structural model for $Sb_x CoSb_{3-x}$ identical to that of cobalt antimonide (i.e., with no guest atom inside the cages). The corresponding charge density map in the inset shows an empty cage. In panel b, the model-free iterative MPF procedure was initiated from the set of structure factors derived from the previous Rietveld analysis exhibited in panel a. In panel c, the same experimental data as in panels a and b was subjected to MEM-based pattern fitting starting from structure factors derived from a model for $Sb_x CoSb_{3-x}$ in which guest Sb atoms partially occupy the 48 h site of space group $Im\bar{3}$, near the center of cage.

allows us to conclude that the samples obtained by processing cobalt antimonide at high pressure and high temperature actually consists of $Sb_x CoSb_{3-x}$, some unmodified $CoSb_3$ and $CoSb_2$. The refinement of XPD data under this assumption leads to a slightly smaller $Sb_x CoSb_{3-x}$ lattice parameter.

Charge density distribution analysis was performed with synchrotron radiation x-ray diffraction data taken at room

temperature for sample #1, according to the MEM-based pattern fitting approach. The evolution of the MPF analysis is shown in Fig. 2. Starting from above, Fig. 2(a) shows the result of a Rietveld analysis in which the high pressure phase $Sb_x CoSb_{3-x}$ was refined using a structural model identical to that of $CoSb_3$, i.e., with empty cages around the $Im\bar{3}$ 2a (0,0,0) site in the skutterudite structure and no vacancies in the framework. One should note the significant difference between experimental and calculated patterns, shown as a red solid line at the bottom. The inset in Fig. 2(a) shows the charge density distribution calculated from the set of structure factors obtained from the Rietveld analysis of data shown in Fig. 2(a). Starting from this set of structure factors calculated for $Sb_x CoSb_{3-x}$, the structural model-free MPF iterative procedure converges with a clear improvement in the agreement between experimental and calculated diffraction patterns, as shown in Fig. 2(b). The 3D charge density distribution, shown in the inset of Fig. 2(b), now exhibits a non-spherical charge buildup around the 2a (0,0,0) site. It is worth to emphasize that this charge buildup around the 2a site resulted from a model-independent iterative MPF analysis which started from a charge density distribution calculated for $Sb_x CoSb_{3-x}$ with empty cages (i.e., from $CoSb_3$, with no bias toward charge accumulation at the center of the cages).

The MPF analysis of synchrotron radiation x-ray diffraction data for the skutterudite phase produced at high pressure and high temperature thus provides further evidence that this phase is formed by the collapse of some atoms from the framework into the cages of the $CoSb_3$ structure. Moreover, the non-spherical shape of the charge density distribution near the center of the cage suggests that, at ambient conditions, the collapsed atom may actually occupy a site near the center of the cage, other than the 2a site.

Accordingly, in order to accelerate the convergence of the iterative MPF process and also to improve the overall agreement between the experimental and calculated synchrotron x-ray diffraction powder patterns, a new MPF analysis was started with a set of structure factors derived from Rietveld analysis of the powder data in which the structure of the high pressure and high temperature phase has guest Sb atoms partially occupying the general site 48 h (x,y,z) near the center of the cage (the Co and Sb atoms in the framework were kept at the 8c and 24 g sites of $Im\bar{3}$ space group, respectively, the latter partially occupied). The structure factors from this Rietveld analysis were taken again as the starting point for a model-free MPF iterative procedure. Figure 2(c) shows the result after convergence of the MPF calculation. Besides the appreciable improvement in reproducing the experimental results, the charge density distribution shown in the inset of Fig. 2(c) now exhibits a set of six maxima off the center of the cage. The total charge inside the cage depicted in the inset of Fig. 2(c), obtained from the sum over the atomic basins in the charge density distribution determined by Bader's analysis, amounts to approximately 50.6*e*. This strongly suggests that Sb atoms from the framework indeed collapses to the interior of the $CoSb_3$ cages, forming a high pressure and high temperature phase that can be retained at ambient conditions, thus giving support to our previous identification of this phase as $Sb_x CoSb_{3-x}$.

The off-center charge distribution depicted in the inset of Fig. 2(c) is consistent with a defect structure formed by the collapse of a Sb atom from the framework inside the cages of the skutterudite structure. In fact, the vacancy left behind by the collapse of a Sb atom breaks the $m\bar{3}$ symmetry of the 2a site at the center of the cage, in such a way that the guest atom is subjected to an anisotropic potential. The antimony atoms that collapse under high pressure and high temperature leave vacancies that are probably distributed among all equivalent positions of Sb in the cage walls, and no particular ordering of the guest atoms is expected in the crystal structure of $Sb_x CoSb_{3-x}$ at ambient conditions. The charge density distribution depicted in Fig. 2(c) thus reflects the distribution of Sb guest atoms into six equivalent sites around the center of the cage, in a way that is consistent with the 12d (x,0,0) site of $Im\bar{3}$ space group. According to Rietveld refinement of the synchrotron XPD data, the distance of the guest Sb atoms from the center of the cages in $Sb_x CoSb_{3-x}$ can be estimated to be around 0.35 Å, at room temperature.

The desinsertion reaction $Sb_x CoSb_{3-x} \rightarrow CoSb_3$ was followed by DSC of sample #2, as represented in Fig. 3. This experiment revealed two thermal events. The first one is a reversible, endothermic event around 150 °C, with an enthalpy of 728 J/mol (corrected for the actual amount of $Sb_x CoSb_{3-x}$ present in the sample). A second run with samples previously heated to 170 °C still exhibits an endothermic peak around 150 °C, only slightly less intense than in the first run. Further cycles of heating (up to 170 °C) and cooling with the same sample revealed that the integrated heat flow of the endothermic peak remains constant from the second run onwards. The second event, an exothermic peak above 180 °C, is related to an irreversible phenomenon whose transition enthalpy is about 21 kJ/mol. No thermal event was observed in the third run, after the sample was heated to 350 °C.

The nature of these two thermal events was further explored by x-ray diffraction analysis of sample #3, after previously heated at different temperatures under a flow of

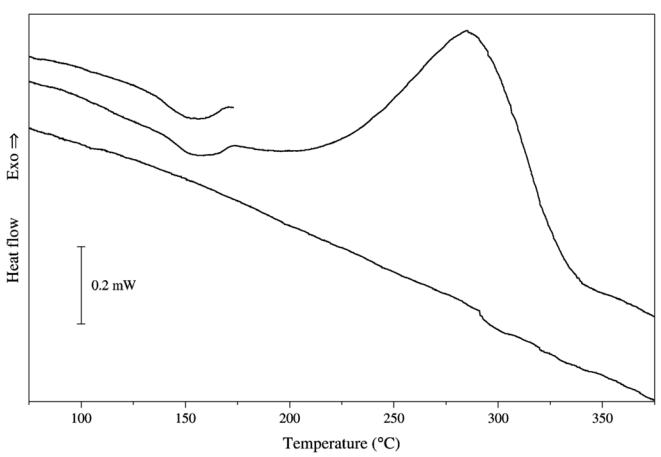

FIG. 3. DSC curves for sample #2 showing, from top to bottom, a small endothermic event near 150 °C in the first heating run up to a maximum temperature of 170 °C (upper curve). The endothermic peak is followed by a large exothermic peak starting at about 180 °C in the second run (middle curve). The third run (bottom curve), shows no sign of the previous thermal events.

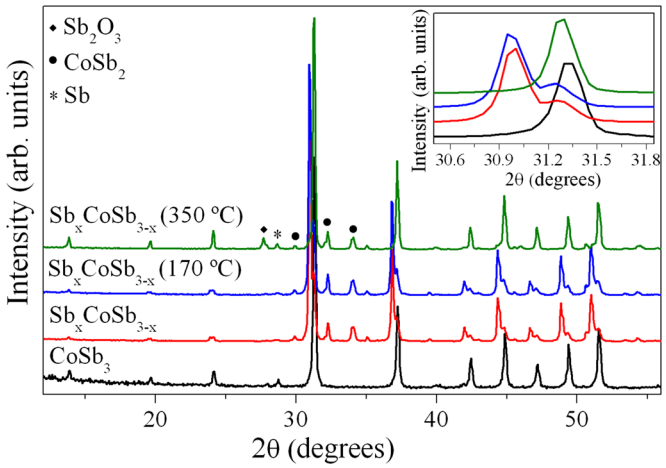

FIG. 4. (Color online) Conventional XRD patterns of sample #3 previously heated at different temperatures and comparison with pristine $CoSb_3$. The inset (in which the XRD patterns are ordered in the same way as in the main graph) shows the disappearance of the 310 Bragg peak from the $Sb_x CoSb_{3-x}$ phase in the XRD data for the sample previously heated to 350 °C. The presence of a minor contamination from Sb_2O_3 is due to residual oxygen in the purge gas used in the thermal treatment of the sample.

ultrapure argon as purge gas, as presented in Fig. 4. The x-ray powder diffraction pattern of pristine $CoSb_3$ was included for comparison. The x-ray diffraction patterns of sample #3 as produced and after previously heated to 170 °C (both measured at ambient conditions) are almost identical, thus confirming that the endothermic event observed at around 150 °C is reversible. On the other hand, the analysis of the x-ray powder diffraction pattern of sample #3, after heated to 350 °C, reveals the disappearance of the Bragg peaks assigned to $Sb_x CoSb_{3-x}$ (see the inset in Fig. 4), thus indicating that the $Sb_x CoSb_{3-x}$ phase was entirely converted back to $CoSb_3$.

From the above reported observations, the exothermic event in the DSC signal can be unambiguously assigned to the desinsertion of antimony atoms from the interior of the $Sb_x CoSb_{3-x}$ skutterudite cages. The kinetics analysis of the DSC signal, according to the method by Borchardt and Daniels, suggests that the desinsertion reaction $Sb_x CoSb_{3-x} \rightarrow CoSb_3$ follows a first-order kinetics, with an activation energy of about 83 kJ/mol.

The observation of Bragg peaks assigned to free Sb in the XRD pattern of sample #3, previously heated to 350 °C, gives further support to the identification of antimony as the guest atom in the high pressure and high temperature skutterudite phase. In fact, this antimony, primarily a part of the $Sb_x CoSb_{3-x}$ phase present in the sample, should be a product of the parallel decomposition reaction $CoSb_3 \rightarrow CoSb_2 + Sb$ that also takes place at high pressure and high temperature. Accordingly, upon desinsertion from $Sb_x CoSb_{3-x}$, the guest antimony atoms made free from decomposition of $CoSb_3$ will remain as free Sb in the sample, as they do not react with $CoSb_2$ to form $CoSb_3$ at such relatively low temperatures.

Room temperature electrical resistivity and lattice parameters measured for sample #4 before and after heat treatments in a vacuum are listed in Table II. There is a relatively small increase of electrical resistivity in samples previously

TABLE II. Room temperature lattice parameter and electrical resistivity for polycrystalline samples of $CoSb_3$ and $Sb_x CoSb_{3-x}$, this latter previously heated to T_{max}. The figures in parentheses are the uncertainties in the last significant digit.

Sample	T_{max} (°C)	$CoSb_3$ a(Å)	$Sb_x CoSb_{3-x}$ a(Å)	ρ ($\mu\Omega \cdot m$)
#4	RT	–	9.125(1)	45(4)
#4	170	–	9.124(2)	76(5)
#4	400	9.038(5)	–	523(6)
$CoSb_3$	RT	9.033(9)	–	818(4)

heated to 170 °C, but the $Sb_x CoSb_{3-x}$ lattice parameter remains identical within the uncertainty of measurement. *In situ* measurements of electrical resistivity at high temperature revealed no abrupt change within the temperature range of the first event observed on DSC analysis (i.e., up to 180 °C). All these observations are in accordance with the results from DSC. Indeed, the first heating to 170 °C may provide enough thermal energy to promote a small fraction of the guest Sb atoms out of the cages. The desinsertion of a small fraction of the guest Sb atoms from $Sb_x CoSb_{3-x}$ may be responsible for the slight reduction of the integrated intensity of the endothermic peak in the second DSC run and, also, for the small increase of room temperature electrical resistivity in samples previously heated to 170 °C. On the other hand, for the sample previously heated above 180 °C, the room temperature electrical resistivity increases toward that of $CoSb_3$, as a consequence of the progress of the desinsertion reaction. It is worth noting the almost twenty-fold increase in room temperature electrical conductivity in going from $CoSb_3$ to $Sb_x CoSb_{3-x}$, which prompts for measurements of thermal conductivity and Seebeck coefficient in order to assess the thermoelectric figure-of-merit for this promising high pressure phase.

To further investigate the nature of the first endothermic event observed in the DSC signal of samples rich in the $Sb_x CoSb_{3-x}$ phase, charge density distribution analysis was performed with synchrotron radiation x-ray diffraction data taken at 155 °C (sample #5). The result of the MPF analysis can be seen in Fig. 2(d). The charge density distribution associated to the guest Sb atom is now evenly spread over about 0.5 Å from the center of the cage, along six equivalent directions. One possible explanation for the shape of the charge density distribution shown in the inset of Fig. 2(d) is that at high temperature, before the onset of the desinsertion reaction, the guest Sb atoms jump from the 12d (x,0,0) to the 2a (0,0,0) site. At the center of the cages, the guest Sb atoms oscillate with high amplitude along the directions dictated by the anisotropic potential to which they are submitted, as the result of the remnant defects on the cage walls. In other words, above 150 °C the guest Sb anisotropic atomic displacement around the equilibrium position at the center of the cage should be very asymmetric and should be oriented along the line that goes from the center of the cage to the defect in the wall left by the atom that collapsed in the self-insertion reaction. The random distribution of these defects among six equivalent directions pointing from the center of the cage thus gives rise to the guest Sb charge distribution

depicted in the inset of Fig. 2(d). The reversible transition of the guest Sb atom from the 12d to the 2a site thus should account for the endothermic peak in the DSC signal at about 150 °C.

IV. CONCLUSIONS

The skutterudite phase obtained by processing $CoSb_3$ at 7.7 GPa and 550 °C was studied by means of conventional and synchrotron radiation x-ray diffraction, DSC and electrical resistivity measurements. The analysis of the charge density distribution for the high pressure and high temperature phase allowed its unambiguous identification as $Sb_x\,CoSb_{3-x}$. Attempts to refine this defect structure according to space group $Im\bar{3}$ have lead to the conclusion that, at room temperature, the guest Sb atoms partially occupy the 12d site, 0.35 Å off the center of the cage in the skutterudite framework. The desinsertion reaction $Sb_x\,CoSb_{3-x} \rightarrow CoSb_3$ at room pressure follows a first-order kinetics, with an onset temperature near 180 °C. The desinsertion reaction is preceded by an endothermic event that was related to the displacement of the guest Sb atoms from the 12d site toward the center of the cage. The room temperature electrical resistivity for samples rich in the self-insertion phase is about 20 times smaller than that of polycrystalline $CoSb_3$. This suggests that measurements of thermal conductivity and Seebeck coefficient should be performed to evaluate the potential of $Sb_x\,CoSb_{3-x}$ as a high performance thermoelectric material.

ACKNOWLEDGMENTS

The authors thank Eduardo Granado (LNLS) for his help in conducting the synchrotron XRD measurements. This work was partially supported by CNPq, CAPES, and LNLS (Brazil).

[1] G. S. Nolas, D. T. Morelli, and T. M. Tritt, Annu. Rev. Mater. Sci. **29**, 89 (1999).
[2] B. C Sales, D. Mandrus, and R. K. Williams, Science **272**, 1325 (1996).
[3] G. Chen, M. S. Dresselhaus, J.-P. Fleurial, and T. Cailat, Int. Mater. Rev. **48**, 45 (2003).
[4] G. S. Nolas, J. Sharp, and H. J. Goldsmid, *Thermoelectrics Basic Principles and New Materials Developments* (Springer, Berlin, 2001).
[5] A. Watcharapasorn, R. C. DeMattei, R. S. Feigelson, T. Caillat, A. Borshchevsky, G. J. Snyder, and J.-P. Fleurial, J. Appl. Phys. **86**, 6213 (1999).
[6] A. Majumdar, Science **303**, 777 (2004).
[7] P. N. Alboni, X. Ji, J. Je, N. Gothard, J. Hubbard, and M. T. Tritt, J. Electron. Mater. **36**, 711 (2007).
[8] G. S. Nolas, J. L. Cohn, and G. A. Slack, Phys. Rev. B **58**, 164 (1998).
[9] B. C Sales, B. C. Chakoumakos, and D. Mandrus, Phys. Rev. B **61**, 2475 (2000).
[10] A. C. Kraemer, M. R. Gallas, J. A. H. da Jornada, and C. A. Perottoni, Phys. Rev. B **75**, 024105 (2007).
[11] A. C. Kraemer, J. A. H. da Jornada, and C. A. Perottoni, Solid State Commun. **133**, 173 (2005).
[12] M. M. Koza, M. R. Johnson, R. Viennois, H. Mutka, L. Girard, and D. Ravot, Nat. Mater. **7**, 805 (2008).
[13] K. Matsui, J. Hayashi, K. Akahira, K. Ito, K. Takeda, and C. Sekine. J. Phys.: Conf. Ser. **215**, 012005 (2010).
[14] B. C Sales, D. Mandrus, B. C. Chakoumakos, V. Keppens, and J. R. Thompson, Phys. Rev. B **56**, 15081 (1997).
[15] F. F. Ferreira, E. Granado, Jr. S. W. Carvalho, D. B. Kycia, and R. Droppa, Jr. J. Synchrotron Radiat. **13**, 46 (2006).
[16] R. A. Young, *The Rietveld Method* (Oxford University Press, Oxford, 1993).
[17] J. Rodriguez-Carvajal, Physica B **192**, 55 (1993).
[18] F. Izumi and K. Momma, Solid State Phenom. **130**, 15 (2007).
[19] F. Izumi and R. A. Dilanian. Recent Res. Dev. Phys. **3**, 699 (2002).
[20] F. Izumi, S. Kumazawa, T. Ikeda, W.-Z. Hu, A. Yamamoto, and K. Oikawa, Mater. Sci. Forum **378**, 59 (2001).
[21] C. J. Howard, J. Appl. Crystallogr. **15**, 615 (1982).
[22] T. Schimidt, G. Kliche, and H. D. Lutz, Acta Crystallogr. C **43**, 1678 (1987).
[23] K. Momma and F. Izumi. J. Appl. Crystallogr. **41**, 653 (2008).
[24] R. F. W. Bader, *Atoms in Molecules - A Quantum Theory* (Oxford University Press, Oxford, 1990).
[25] H. J. Borchardt and F. Daniels, J. Am. Chem. Soc. **79**, 41 (1957).
[26] V. S. Kumar, G. Kelekanjeri, and R. A. A. Gerhardt, Meas. Sci. Technol. **19**, 1 (2008).
[27] H. Takizawa, K. Miura, M. Ito, T. Suzuki, and T. Endo, J. Alloy. Compd. **282**, 79 (1999).